

Valence-bond solid as the quantum ground state in honeycomb layered urusovite $\text{CuAl}(\text{AsO}_4)\text{O}$ A. N. Vasiliev,^{1,2,3,*} O. S. Volkova,^{1,2} E. A. Zvereva,¹ A. V. Koshelev,¹ V. S. Urusov,¹ D. A. Chareev,⁴ V. I. Petkov,⁵ M. V. Sukhanov,⁵ B. Rahaman,⁶ and T. Saha-Dasgupta⁷¹*Lomonosov Moscow State University, Moscow 119991, Russia*²*Ural Federal University, Ekaterinburg 620002, Russia*³*National University of Science and Technology "MISIS," Moscow 119049, Russia*⁴*Institute of Experimental Mineralogy, Russian Academy of Sciences (RAS), Chernogolovka, Moscow Region 142432, Russia*⁵*Lobachevsky State University of Nizhny Novgorod, Nizhny Novgorod 603950, Russia*⁶*Aliah University, Kolkata 700156, India*⁷*S. N. Bose National Centre for Basic Sciences, Kolkata 700098, India*

(Received 27 November 2014; revised manuscript received 20 March 2015; published 7 April 2015)

The synthetic mineral urusovite $\text{CuAl}(\text{AsO}_4)\text{O}$ was prepared through the wet chemistry route and characterized over a wide temperature range in terms of studies of magnetization, specific heat, and X-band electron spin resonance. The basic structural units of the compound are distorted square pyramids CuO_5 assembled into corrugated honeycomb layers separated by AsO_4 and AlO_4 tetrahedrons. Both thermodynamic and resonant measurements indicate that $\text{CuAl}(\text{AsO}_4)\text{O}$ is a spin gap system with a gap of ~ 350 K. The electronic structure calculations performed within the framework of density functional theory suggest a weakly interacting dimer model with antiferromagnetic signs for both intradimer and interdimer superexchange interactions. This establishes the valence bond solid as the quantum ground state of the title compound. The pronounced discrepancy between experimental data and calculations within the weakly interacting dimer model at elevated temperatures is ascribed in part to the steep increase of the intradimer exchange interaction parameter driven by the thermal expansion effects.

DOI: [10.1103/PhysRevB.91.144406](https://doi.org/10.1103/PhysRevB.91.144406)

PACS number(s): 75.10.Kt, 75.30.Et, 75.40.Cx

I. INTRODUCTION

The urusovite with the chemical formula $\text{CuAl}(\text{AsO}_4)\text{O}$ is a newly found mineral among products of volcanic exhalations of the great Tolbachik fissure eruption in 1975 at Kamchatka, Russia [1]. The temperature of the locality where the sample was found was $\sim 400^\circ\text{C}$ (700 K), which explains the absence of the hydroxyl groups or water molecules inevitably present in the crystal structure of numerous naturally occurring compounds with a spin gap behavior. A variety of mechanisms were found to be responsible for the spin gap formation with similar magnitudes, such as found in (1) the libethenite $\text{Cu}_2\text{PO}_4(\text{OH})$, described by an isolated square-spin cluster model [2]; (2) the malachite $\text{Cu}_2(\text{OH})_2\text{CO}_3$, representing weakly interacting alternating spin chains [3,4]; (3) the clinoclase $\text{Cu}_3(\text{AsO}_4)(\text{OH})_3$, being a combination of two nonequivalent spin dimers [5]; and (4) the euchroite $\text{Cu}_2(\text{AsO}_4)(\text{OH}) \times 3\text{H}_2\text{O}$, a model compound for the frustrated delta chain composed of corner-sharing triangles [6]. An introduction to the variety of peculiar magnetic phenomena observed in Cu-based minerals is provided in Ref. [4]. Unlike the other listed compounds, the greater chemical stability of $\text{CuAl}(\text{AsO}_4)\text{O}$ opens a perspective to studying the physical properties of a large spin gap compound in a significantly wider temperature range.

II. EXPERIMENTAL DETAILS

To synthesize $\text{CuAl}(\text{AsO}_4)\text{O}$, a mole of an $\text{Al}(\text{NO}_3)_3$ water solution was mixed with a solution of $\text{Cu}(\text{NO}_3)_2$ obtained

through the reaction of CuO with concentrated nitric acid. Then, the half-mole of arsenic acid H_3AsO_4 was added to the mixture. The arsenic acid was obtained at heating by oxidation of elementary arsenic in a mixture of nitric and hydrochloric acids in an equal volume ratio. The product obtained was dried at 90°C and 250°C and thermally treated in air at 600°C , 800°C , and 1000°C for 24 h. The step-by-step heating was alternated with fine grinding in an agate mortar to secure the sample's homogenization. At every stage of the synthesis, the phase composition was controlled by x-ray diffraction (XRD-6000, Cu K_α radiation, 2θ range 10° – 60°). According to x-ray analysis, the sample fired at 600°C contains mostly the AlAsO_4 phase with space group $P3_121$. The annealing at 800°C resulted in the formation of the title compound, as shown in Fig. 1, while further increase of temperature to 1000°C led to improved crystallization of the phase. The parameters of the primitive cell at room temperature were determined as $a = 7.3266(2)$, $b = 10.2427(3)$, $c = 5.5946(3)\text{Å}$, $\beta = 99.808(2)^\circ$, $Z = 4$, and space group $P2_1/c$.

The urusovite $\text{CuAl}(\text{AsO}_4)\text{O}$ has a monoclinic primitive cell with four formula units per unit cell. The basic structural unit consists of the Cu atom in the center of a distorted oxygen pyramid. The Cu-O bond lengths range from 1.96 to 2.73 Å with an average value of 2.05 Å. Two neighboring CuO_5 pyramids share a common edge to form a dimer unit, while two such neighboring units share a common corner in the bc plane and form a honeycomblike structure, as shown in the right panel of Fig. 2. Two such layers of honeycomb are connected via AsO_4 and AlO_4 tetrahedrons, as shown in the left panel of Fig. 2. The bc planes containing honeycomb structures are stacked on top of each other along the a direction.

*Corresponding author: vasil@lt.phys.msu.ru

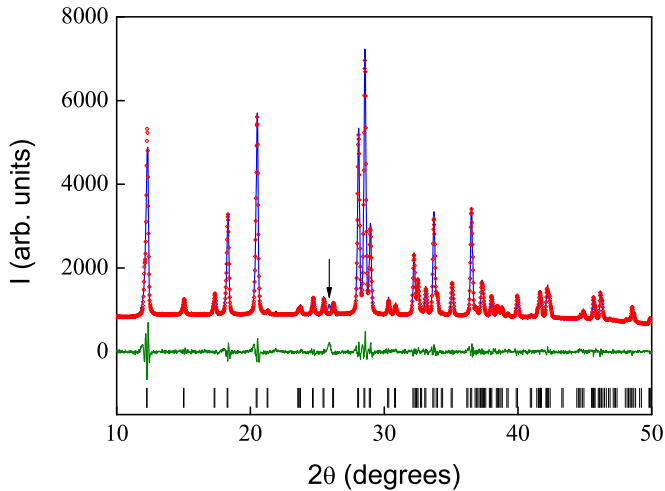


FIG. 1. (Color online) The x-ray patterns of the powder sample of $\text{CuAl}(\text{AsO}_4)\text{O}$ collected at $T = 300$ K plotted in comparison with the pattern obtained from a profile refinement (solid blue line). The difference is shown in the lower part of the figure by the green solid line. The positions of the Bragg reflections used to simulate the patterns are indicated by the small vertical bars in the lower part. The black arrow indicates the main peak of the AlAsO_4 secondary phase.

Electron spin resonance (ESR) studies were carried out using X-band ESR spectrometer CMS 8400 (ADANI) ($f \approx 9.4$ GHz, $B \leq 0.7$ T) equipped with a low temperature mount operating in the range $T = 5$ –300 K. The effective g factor has been calculated with respect to the a , g -bis(diphenyl)- b -phenylallyl (BDPA) reference sample with $g_{\text{eff}} = 2.00359$.

The field and temperature dependences of the magnetization in $\text{CuAl}(\text{AsO}_4)\text{O}$ were measured in the temperature range 2–1000 K and in magnetic field B up to 9 T by means of a Physical Property Measurement System (PPMS-9T, Quantum Design). The specific heat data were obtained by a relaxation technique in that same system in the temperature range 2–390 K on a sample with a mass of ~ 10 mg.

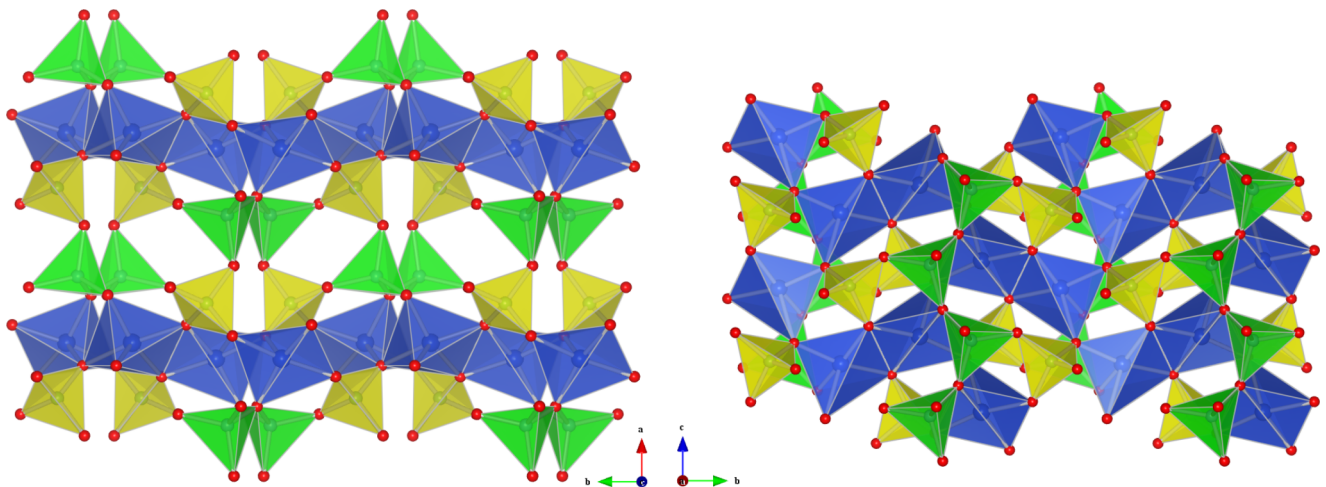


FIG. 2. (Color online) The crystal structure of the urusovite $\text{CuAl}(\text{AsO}_4)\text{O}$ in polyhedral representation in (left panel) the ab plane and (right panel) the bc plane. The corrugated layers of edge-sharing and corner-sharing CuO_5 pyramids (blue) are separated by AlO_4 (green) and AsO_4 (yellow) tetrahedra.

III. RESONANCE PROPERTIES

The evolution of ESR spectra with temperature in the powder sample of $\text{CuAl}(\text{AsO}_4)\text{O}$ is shown in Fig. 3. One can distinguish two principally different regions over the temperature range studied. At high temperatures ($T \geq 90$ K), an almost isotropic single broad absorption line ascribable to Cu^{2+} ions is observed. Its amplitude passes through maximum and then decreases with decreasing temperature. Further decrease of the temperature leads to significant changes in the character of the ESR spectra, and a strongly anisotropic absorption line with a visible hyperfine structure ($T \leq 60$ K) is observed.

Since the resonant signal is relatively broad at high temperature (the same order as the resonance field), two circular components of the exciting linearly polarized microwave field have to be taken into account. Therefore, for analysis, the ESR signals on both sides of $B = 0$ have to be included into the fitting formula, which has been taken in a conventional form:

$$\frac{dP}{dB} \propto \frac{d}{dB} \left[\frac{\Delta B}{\Delta B^2 + (B - B_r)^2} + \frac{\Delta B}{\Delta B^2 + (B + B_r)^2} \right] \quad (1)$$

This formula describes a symmetric line, where P is the power absorbed in the ESR experiment, B_r is the resonance field, and ΔB is the linewidth. The results of ESR lineshape fitting are shown by the solid lines in Fig. 3 (left panel).

It is natural to expect a powderlike spectrum for a powder sample of a paramagnet with magnetic Cu^{2+} ions. Indeed, this kind of spectrum was observed at low temperature due to impurity, as presented in Fig. 3 (right panel). The width of the band of absorption, arising due to the distribution of effective g factors in different microcrystals between the values of g_{\perp} and g_{\parallel} , is 50 mT. The linewidth of the ESR signal recorded at high temperatures is three times larger—about 150 mT. Thus, the large linewidth could mask the bandwidth of absorption of the powder sample considered without natural broadening. In addition, we are dealing with a dimer system, and the different Cu spins in the dimer, which are strongly coupled by a large exchange interaction, have different ligand fields

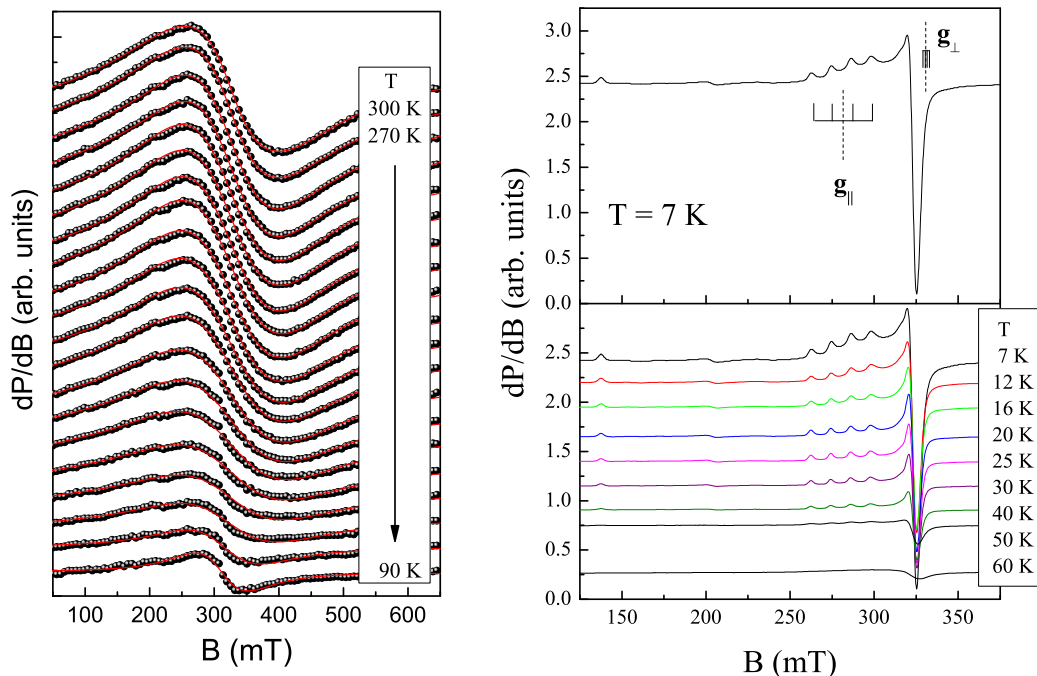


FIG. 3. (Color online) Temperature dependences of the X-band ESR signal (left panel) from the matrix and (right panel) from the impurities/defects in $\text{CuAl}(\text{AsO}_4)\text{O}$.

(namely, different anisotropic environments), thus causing the isotropic g value. These may be the reasons for the absence of visible manifestation of the powder-type absorption band in the temperature range above 90 K, and we could fit experimental data by a Lorentzian function for quantitative estimations.

Apparently, the fitted curves are in good agreement with the experimental data. The temperature dependencies of the effective g factor, the linewidth ΔB , and the integral ESR intensity χ_{ESR} (which is proportional to the number of magnetic spins) as derived from this fitting procedure are summarized in Fig. 4. The average effective g factor at room temperature is found to be $g = 2.05$ (upper panel in Fig. 4), which is a reasonable value for Cu^{2+} ions in the pyramidal coordination [7]. This value is influenced by internal magnetic field in the matrix, however. With lowering of the temperature, the measured g factor remains essentially independent of temperature down to ~ 90 K; afterwards, it shifts to higher values. This shift is the artifact related to switching of the main ESR signal from the matrix to the impurity. The linewidth demonstrates nonmonotonic behavior, indicating different spin-dynamic regimes over the temperature range under study (middle panel in Fig. 4). At high temperatures ($T > 200$ K) the linewidth remains almost constant, which is typical for an exchange-narrowed ESR absorption line. Decreasing the temperature below ~ 200 K leads to a slow increase of the linewidth, which is due to development of short-range magnetic correlations, tentatively. It passes through a smooth maximum at $T \sim 130$ K, which may reflect a saturation of spin correlation length, and then it decreases progressively down to ~ 70 K, when the ESR signal from the matrix vanishes eventually. Similar behavior was found earlier for the spin gap compound $\eta\text{-Na}_{1.286}\text{V}_2\text{O}_5$ and interpreted based on the concept of memory function $F(T)$, which is

the sum of spin correlation functions. The linewidth in this approach is proportional to the memory function $F(T)$ divided

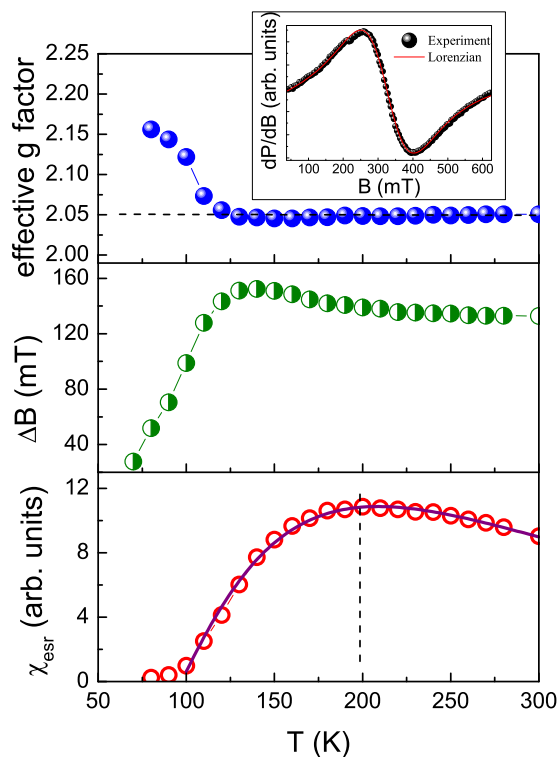


FIG. 4. (Color online) The temperature dependences of the main ESR parameters of the matrix of $\text{CuAl}(\text{AsO}_4)\text{O}$: (upper panel) the effective g factor, (middle panel) the linewidth ΔB , and (lower panel) the intensity χ_{ESR} . Inset: The first derivative of the ESR absorption line at $T = 200$ K. Circles are experimental data, and the red solid line is the fitting to the Lorentzian profile.

by $\chi_0(T) \times T$. This, for instance, leads to linear dependence of ΔB vs T (Oshikawa-Affleck law) in the case of $S = 1/2$ antiferromagnetic (AFM) Heisenberg chain when $F(T) \sim T^2$. At the same time, in the case of spin gap systems, one would expect a more rapid decrease of ΔB with temperature [8]. So, narrowing of the line below ~ 130 K might be interpreted as a strong depletion of the spin fluctuation density due to the opening of the spin gap. The integral ESR intensity (lower panel in Fig. 4) passes through a broad smooth maximum when the temperature decreases, indicating clear low dimensional behavior as expected for the dimer system.

For the dimer system, the signal observed can be related to that from the interacting pairs S_i and S_j with effective spin $S = 1$. The singlet is ground state with the triplet level lying ~ 350 K above (this intradimer exchange coupling is estimated in the next section and corresponds on a frequency scale to ~ 500 cm $^{-1}$ or ~ 15 000 GHz). Spectra of pairs in the strong exchange limit are generally formed by one or more spectra arising by the spin multiplets that are thermally populated, in our case from triplet one. In its turn, single ion zero-field splitting can be fairly large in the pairs of transition metal ions even in the case of orbitally nondegenerate ground states, and it can remove degeneracy of the triplet state. In addition, when the spin centers are equal, the g tensor of the pair will be identical to the tensors of the individual spins S_i and S_j . However, if two individual g tensors are different, the g tensor of the pair may be remarkably different from each of them. It must be recalled that “different” also means two identical but differently oriented tensors. In our case, the dimers are formed by two differently oriented tensors along the c axis pyramids CuO $_5$, which are edge shared in the square basal plane (right panel of Fig. 2).

At temperatures below 60 K, there is another ESR signal that might be related to the presence of impurity/defects; two very weak additional resonance modes at low fields are also visible. The ESR powder pattern is characteristic of Cu $^{2+}$ ions with an anisotropic g tensor. The intensity of this signal increases with lowering of the temperature in accordance with

the Curie-Weiss law. The presence of paramagnetic impurities was also detected in the static magnetic susceptibility data. In addition, the well-resolved anisotropic hyperfine structure appears at low temperatures due to interaction between the electron magnetic moment of the unfilled electron d shell of Cu $^{2+}$ ions and the nuclear magnetic moment of the ^{63}Cu ($I = 3/2$, natural abundance 69%) and ^{65}Cu ($I = 3/2$, natural abundance 31%) isotopes. Both principal components of the g tensor remain almost temperature independent in the T range of 7–60 K and were determined from the parallel and perpendicular components of the hyperfine structure. On average, $g_{\parallel} = 2.37 \pm 0.01$ and $g_{\perp} = 2.02 \pm 0.01$, resulting in an effective g factor = 2.14. The hyperfine interaction constants were estimated to be about $^{63,65}A_{\parallel} \approx 381$ MHz and $^{63,65}A_{\perp} \approx 34$ MHz, respectively.

IV. THERMODYNAMIC PROPERTIES

The temperature dependence of magnetic susceptibility χ taken in the range 2–1000 K at $B = 1$ T in CuAl(AsO $_4$)O is shown in Fig. 5 (left panel). At low temperatures, it shows the prevailing contribution of the impurities/defects related term; the magnetic susceptibility passes through the broad maximum below room temperature and somewhat nonmonotonously decreases at elevated temperatures. To reveal the matrix contribution, the measurements of χ were repeated also at the highest available field $B = 9$ T in the range 2–400 K, as shown in the inset to Fig. 5 (left panel). At $T_{\text{max}} \sim 215$ K, the magnetization passes through broad maximum and decreases progressively with increasing temperature. The $\chi(T)$ dependence taken at $B = 1$ T was fitted in the range 2–1000 K by the formula for the noninteracting dimers with inclusion of the temperature independent term and the impurities/defects related term:

$$\chi = \chi_0 + \frac{C_{\text{imp}}}{k_B T} + \frac{N_A \mu_B^2 g^2}{k_B T [3 + \exp(J_1/k_B T)]} \quad (2)$$

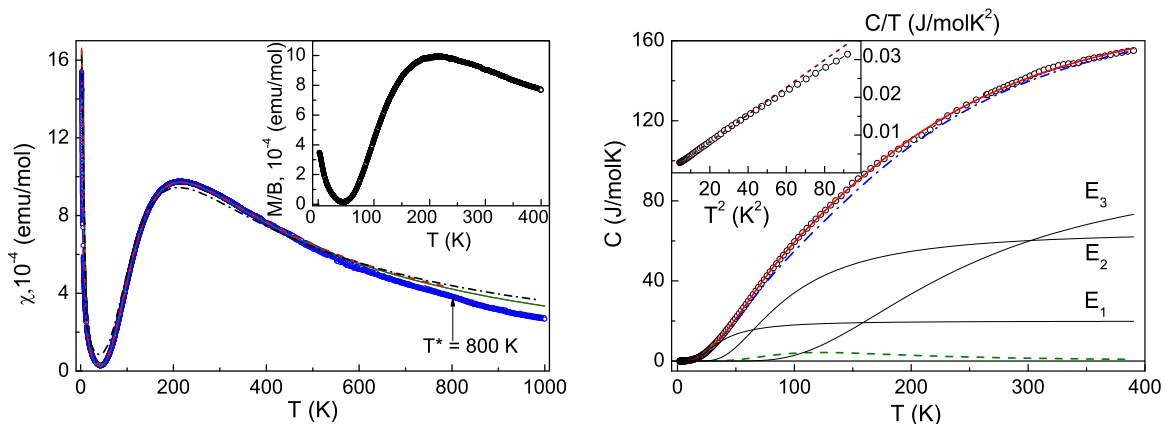


FIG. 5. (Color online) (left panel) The temperature dependence of magnetic susceptibility in the urusovite CuAl(AsO $_4$)O taken at $B = 1$ T. The solid line in the range 2–1000 K represents the fit in the model of noninteracting dimers. The dashed line represents the fit in the range 2–800 K. The dashed-dotted line represents the fit with the fixed value of the g factor = 2.05. The inset represents the M/B vs T dependence taken at $B = 9$ T. (right panel) The temperature dependence of the specific heat in the urusovite CuAl(AsO $_4$)O (symbols). The dashed line represents the magnetic dimers’ contribution. The dashed-dotted line represents the lattice contribution described by the sum of three Einstein functions E_1 , E_2 , and E_3 . Inset: C/T vs T^2 dependence (symbols) and the fit of low temperature data by the Debye T^3 law (dashed line).

where N_A , μ_B , and k_B are Avogadro, Bohr, and Boltzmann constants, respectively. The fit is shown by the solid line in Fig. 5 (left panel).

Equation (2) contains four independent parameters, i.e., $\chi_0 \approx -7.9 \times 10^{-5}$ emu/mol, which represents the temperature independent contribution; the defects/impurities concentration $C_{\text{imp}} = 0.0034$ emu/mol K; the g factor of Cu^{2+} ions $g = 2.185$, which differs from the value of the g factor estimated in the ESR study around room temperature; and $J_1 = 350 \pm 5$ K, the intradimer exchange interaction parameter equal to the gap Δ in the spectrum of magnetic excitations. The fitting with the fixed g value = 2.05, which was determined from the ESR data, results in a significantly worse description of the experimental data (black dashed-dotted curve in the left panel of Fig. 5) but leads to a similar estimation for the spin gap $\Delta = 342 \pm 5$ K. This is to be expected since the g value evaluated in the ESR measurements differs from that for “noninteracting” Cu^{2+} ions. The temperature independent term represents the summation of diamagnetic Pascal’s constants of individual ions [9] in the chemical formula of $\text{CuAl}(\text{AsO}_4)\text{O}$ and the paramagnetic van Vleck term [10] associated with splitting of the d shell of Cu^{2+} ions. The fitting of the integral ESR intensity according to the third term of Eq. (2), i.e., within the frame of the simple dimer model, results in a good description of the experimental ESR data with $g = 2.05$ and an almost similar estimation for the spin gap parameter $\Delta_{\text{ESR}} = 345 \pm 5$ K as obtained from static magnetic susceptibility; the fitting curve is shown by the solid line in the lower panel of Fig. 4. Above $T^* \sim 800$ K, the derivative $d\chi/dT$ increases somewhat, indicating further deviations from the fitting curve, as shown in Fig. 5 (left panel). The fit by Eq. (2) in the range 2–800 K, shown by the dashed line in Fig. 5 (left panel), gives essentially the same values for every independent parameter.

The title compound is chemically stable at ambient air pressure up to 1000 °C. The measurements of magnetic susceptibility were performed, however, under conditions of dynamic high vacuum. In this case, the partial decomposition of the sample into AlAsO_4 and CuO phases can occur, as was confirmed by independent XRD study. While the measurements of magnetic susceptibility on the fresh samples are quite reproducible, the repeatable measurements on the same sample lead to systematic lowering in the measured values of χ above $T^* = 800$ K.

The temperature dependence of specific heat C in $\text{CuAl}(\text{AsO}_4)\text{O}$ is shown in Fig. 5 (right panel). No indication of the phase transitions is found in the temperature range measured. The value of spin gap Δ estimated in magnetic susceptibility measurements was used to calculate the temperature dependence of magnetic specific heat in accordance with the formula [11]

$$C = \frac{3}{2}R \left(\frac{\Delta}{k_B T} \right)^2 \exp(-\Delta/k_B T) / (1 + 3 \exp(-\Delta/k_B T)) \quad (3)$$

where $R = 8.314$ J/molK is the universal gas constant. These data are shown by the dashed line in Fig. 5 (right panel). The extraction of the magnetic contribution from the total

specific heat gives the lattice contribution C_{lat} , shown by the dashed-dotted line in Fig. 5 (right panel).

The lattice contribution could be described by three Einstein functions with energy $E_1 = 112$ K, $E_2 = 287$ K, and $E_3 = 763$ K. Tentatively, these values correspond to lattice vibrations within three rigid structural units in $\text{CuAl}(\text{AsO}_4)\text{O}$, i.e., CuO_5 pyramids and AsO_4 and AlO_4 tetrahedra. In a wide temperature range, the Einstein model describes the experimental data surprisingly well, taking into account its simplicity. At the same time, the significantly more elaborate Debye model or Born–von Karman theory [12] fails in fitting the low temperature specific heat, as shown in the inset to Fig. 5 (right panel). As the temperature increases, the experimental data strongly deviate downward from the Debye T^3 law. Therefore, in the frame of this approach, the overall fit of the experimental data in the range 2–390 K is rather poor. It must be recalled, however, that the Debye model assumes an ideal solid. In polycrystalline materials, the impurities and defects, as well as the grain boundaries, may significantly complicate C vs T dependence, resulting in multiple Schottky-type anomalies. The presence of an appreciable number of defects in urusovite stems from the low temperature upturn of magnetic susceptibility.

V. FIRST PRINCIPLES CALCULATIONS

Electronic structure calculation has been carried out for the urusovite $\text{CuAl}(\text{AsO}_4)\text{O}$ with an aim to figure out the underlying spin model. Calculations have been carried out within the framework of density functional theory (DFT) [13] within the generalized gradient approximation [14] for the exchange-correlation functional. The magnetic interactions have been computed using the superexchange formula [15] and the knowledge of effective hopping interactions, as given by the muffin-tin orbital (MTO) based N th-order MTO (NMTO) downfolding calculation [16].

The Cu-O bond lengths of the distorted pyramid and the various angles are shown in Fig. 6 (left panel). The splitting of the d shell of Cu in a pyramidal environment at room temperature is shown in Fig. 6 (right panel). A non-spin-polarized self-consistent calculation has been carried out for the compound. The calculated electronic density of states is presented in Fig. 7 (left panel). The pyramidal environment of oxygen atoms surrounding Cu results in the $\text{Cu } d_{x^2-y^2}$ state at the Fermi level pronouncedly mixed with O p states. A small admixture of the Al p and As p states is also found at the Fermi level, which mediates interactions from one layer to another layer in the compound. With Cu being in the 2+ oxidation state, all d states are completely filled except for the $d_{x^2-y^2}$ state, which is half filled. Therefore, the Cu $d_{x^2-y^2}$ state at the Fermi level is primarily responsible for the electronic and magnetic behavior of the compound.

The corresponding spin-polarized density of states, obtained in a self-consistent spin-polarized DFT calculation and projected onto the Cu d , O p , Al p , and As p states, is shown in Fig. 7 (right panel). We find that the pyramidal crystal field splits the Cu d levels according to the scheme shown in Fig. 6 (right panel). All d states are completely filled in the majority and minority spin channels except for the minority channel of Cu $d_{x^2-y^2}$, suggesting the nominal Cu^{2+} or d^9

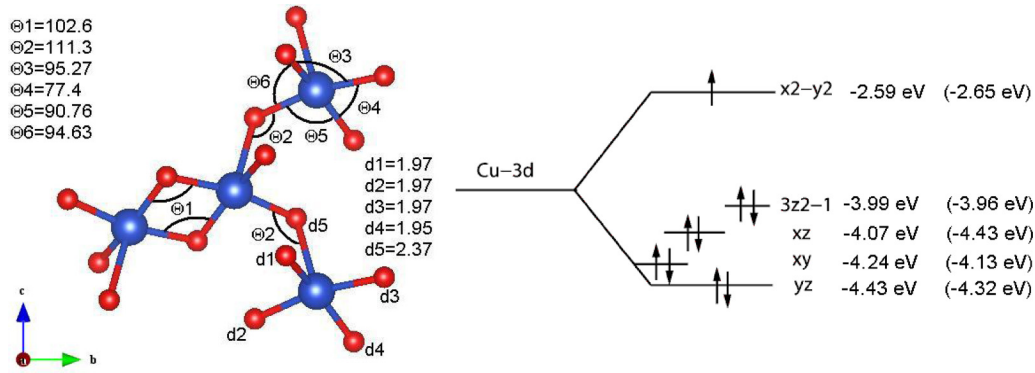


FIG. 6. (Color online) (left panel) The various Cu-O distances and angles within a CuO₅ pyramid and between the pyramids in CuAl(AsO₄)O at room temperature. (right panel) Crystal field splitting of the Cu *d* shell in the pyramidal environment at room temperature. The data for 1000 K are given in parentheses.

valence of Cu. Both Al *p* and As *p* are found to be nearly empty, suggesting the nominal Al³⁺ and As⁵⁺ valences, while the O *p* states are found to be mostly occupied, suggesting the nominal 2- valence states. The O *p* states show finite, nonzero hybridization with the Cu *d* states close to Fermi energy, which contributes to the superexchange path of magnetic interaction between two Cu sites. The calculated magnetic moment at a Cu site is found to be 0.67 μ_B, with the rest of the moment sitting at the neighboring O site and with a total magnetic moment of ~1 μ_B per formula unit.

In order to estimate the various Cu-Cu magnetic exchange interactions present in the compound, the NMTO based downfolding technique was applied to construct Cu *d*_{x²-y² only Wannier functions by downfolding all degrees of freedom associated with O, Al, As, and Cu and keeping active only the Cu *d*_{x²-y² degrees of freedom. This procedure provides renormalization of Cu *d*_{x²-y² orbitals due to hybridization from O *p*, Al *p*, and As *p* and from the other Cu *d* orbitals. The effective Cu *d*_{x²-y² - Cu *d*_{x²-y² hopping interactions were obtained from the real space representation of the Hamiltonian in the effective Cu *d*_{x²-y² Wannier function basis. The dominant hopping interaction is found to be the nearest neighbor in-plane interaction *t*₁ = 261 meV. The next nearest neighbor in-plane interaction *t*₂ is found to be 9.5 meV, much smaller compared to}}}}}}

*t*₁. The interaction between the planes *t*₃ is found to be 40 meV. The Cu²⁺ ions, therefore, exhibit a dimer-type interaction. The magnetic interactions *J*₁, *J*₂, and *J*₃ can be obtained from the knowledge of hopping interactions with a choice of the Hubbard *U* parameter by using the superexchange formula 4*t*²/*U*. The paths for dominant magnetic interactions are shown in Fig. 8. We see that *J*₁ is mediated by the Cu *d*-O *p*-Cu *d* superexchange path, where the Cu-O-Cu bond angle is 102.6°, while *J*₂ is mediated by the Cu *d*-O *p*-Cu *d* superexchange path, where the Cu-O-Cu bond angle is 111.3°, and *J*₃ is mediated by the Cu *d*-O *p*-Al *p*-O *p*-As *p*-O *p*-Cu *d* super-superexchange path between the layers. The interaction *J*₁, mediated by the edge shared superexchange path via O, turned out to be the strongest, whereas the interaction *J*₂, which is mediated by the corner shared superexchange path via O, is found to be much smaller compared to *J*₁. The interaction *J*₃, mediated by the corner shared super-superexchange path via O, Al, O, As, O, is found to be smaller than *J*₁ but larger than *J*₂. At room temperature, the values turned out to be *J*₁ = 350 K, *J*₂ = 0.6 K, and *J*₃ = 8.3 K, with a choice of *U* = 9 eV. The positive signs for all interactions indicate the AFM nature of exchange interactions. The calculations thus suggest a very weakly interacting dimer model, as shown in Fig. 9.

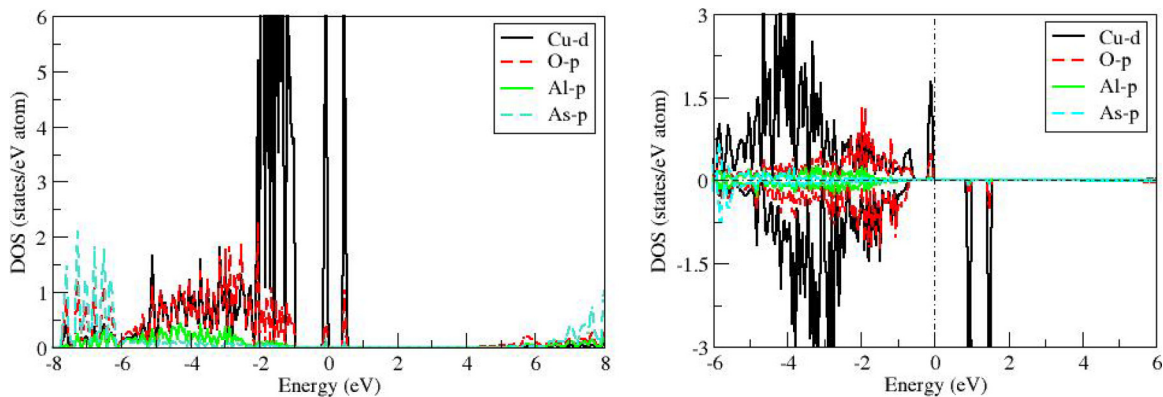


FIG. 7. (Color online) (left panel) Electronic density of states calculated using DFT in CuAl(AsO₄)O. The energy axis is plotted with respect to the Fermi energy. (right panel) The spin-polarized density of states. The up channel of Cu *d* is completely filled, while the down channel of Cu *d* is partially filled.

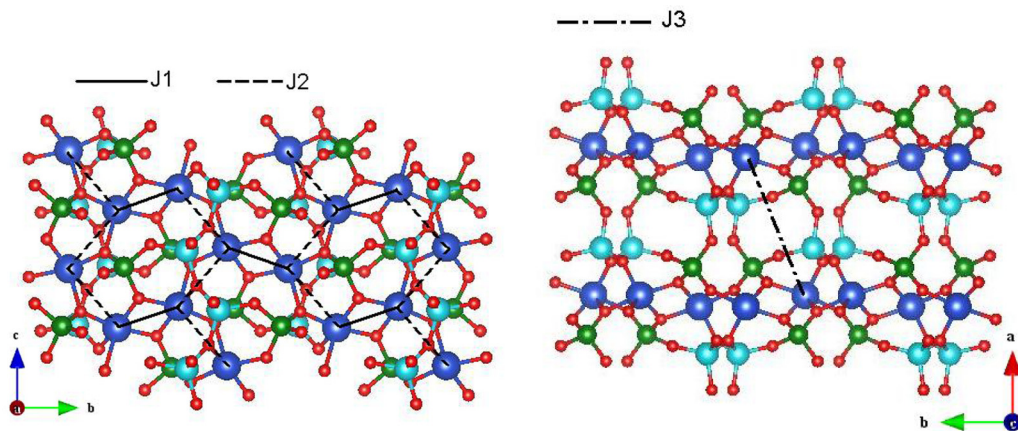


FIG. 8. (Color online) (left panel) The exchange paths for various magnetic interactions J_1 (solid line) and J_2 (dashed line). (right panel) The exchange paths between two honeycomb layers mediated by AsO_4 and AlO_4 tetrahedra, J_3 (dashed-dotted line).

Since the experimental study of magnetic susceptibility was extended up to 1000 K, we calculated the magnetic exchange parameters for the relaxed structure of urusovite at this temperature. The thermal expansion of $\text{CuAl}(\text{AsO}_4)\text{O}$, as measured in Ref. [1], leads to pronounced changes in interatomic distances and bond angles, as shown in Table I. Most spectacular is the increase of the bond angle θ_1 for Cu-O-Cu intradimer superexchange interaction, which rises from 102.36° to 105.38° . At 1000 K, the values turned out to be, $J_1 = 535$ K, $J_2 = 5$ K, and $J_3 = 5$ K, with a choice of $U = 9$ eV. Besides, the thermal expansion effects lead to changes in the crystal field splitting scheme of the Cu d shell in the pyramidal environment, as shown by the values in parentheses in Fig. 6 (right panel). The nearest and next nearest neighbor exchanges on a variety of copper oxide compounds have been studied in the literature [17] using an exact diagonalization technique on small CuO clusters. The paper showed crucial dependence of the Cu-O-Cu angle on the magnetic exchanges through changes in hopping interactions, as found in the present paper. As mentioned, the thermally induced structural changes also change the crystal field splitting, which provides another source for changing

the strength of magnetic exchanges by changing the charge transfer energy.

VI. DISCUSSION

The temperature range of experimental study of the magnetic susceptibility in the urusovite $\text{CuAl}(\text{AsO}_4)\text{O}$ was significantly wider than in routine practice [18–22]. The measurements up to room temperature usually do not need to take into account the effects associated with the temperature expansion. At elevated temperatures, however, the changes in interatomic angles and distances can result in drastic alternations of the exchange interaction parameters. Besides, the splitting of the d shell of transition metal can be modified with temperature, resulting in changes of the g factors and van Vleck contribution [23]. While the estimation of the g factors requires information on the strength of the spin-orbit interaction, the van Vleck contribution can be estimated based on the splitting of the Cu d shell at various temperatures.

The discrepancy between the experimental data and the fitting curve reaches $\sim 10\%$ at 800 K and 25% at 1000 K. One can consider various physical and chemical factors as responsible for this discrepancy.

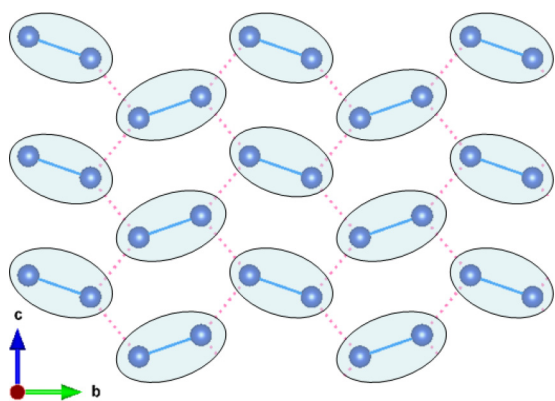


FIG. 9. (Color online) The valence bond solid representation of the magnetic subsystem of the urusovite $\text{CuAl}(\text{AsO}_4)\text{O}$ on the background of distorted honeycomb lattice.

TABLE I. Interatomic distances and bond angles in relaxed crystal structure of urusovite $\text{CuAl}(\text{AsO}_4)\text{O}$, as shown in Fig. 6 (left panel).

Bond angles (θ , $^\circ$) distances (d , \AA)	$T = 300$ K	$T = 1000$ K
θ_1	102.36	105.38
θ_2	111.32	112.62
θ_3	101.07	101.67
θ_4	77.64	74.62
θ_5	90.48	91.68
θ_6	94.88	95.87
d_1	1.97	1.956
d_2	1.967	1.955
d_3	1.97	1.962
d_4	1.96	1.967
d_5	2.37	2.306

The van Vleck contribution to the magnetic susceptibility can be written as

$$\chi_{vV} = \frac{4N_A\mu_B^2}{\Lambda} \quad (4)$$

where $\Lambda = |10Dq|$ is the energy separation of the d orbital states in a pyramidal crystal field. While the redistribution of energy levels with temperature takes place, as shown in Fig. 6, the overall splitting of the Cu d shell changes modestly, resulting in reduction of the paramagnetic contribution, i.e., $\chi_{vV} = 7.47 \times 10^{-5}$ emu/mol at 300 K and 7.26×10^{-5} at 1000 K. While of the proper sign, the difference of 3% does not allow an explanation of the discrepancy between the experimental data and the fitting curve.

Another factor influencing the absolute values of χ is the presence of interdimer interactions taken with appropriate multiplicities. The fitting of the experimental data with a large number of independent variables is nonproductive, resulting sometimes in similarly good fits for different sets of parameters. To take into account intraplane J_2 and interplane J_3 , exchange interactions between dimers is possible based on the values estimated in first principles calculations. This can be done using the formula

$$\chi = \chi_0 + \frac{C_{\text{imp}}}{k_B T} + \frac{N\mu_B^2 g^2}{k_B T [3 + \exp(J_1/k_B T) + J^*/k_B T]} \quad (5)$$

where the summary interdimer interaction $J^* = 2J_2 + J_3$ comprises 9.5 K at room temperature and 15 K at the highest temperature of the present paper. This factor alone reduces the magnetic susceptibility at elevated temperatures by less than 1%.

The most important factor appears to be the increase of the intradimer exchange interaction parameter J_1 from 350 K at room temperature up to 535 K at the highest temperature of the present paper. This factor alone results in a 10% reduction of magnetic susceptibility being the main physical reason of the discrepancy between the measured data and the fitting curve. The rest we have to attribute to chemical decomposition of the title compound above T^* . The

discrepancy between the experimental data at elevated temperatures and the fitting curves becomes even more pronounced when using the reduced value of the g factor estimated in ESR measurements.

VII. CONCLUSION

The combined experimental and theoretical studies of the newly found mineral urusovite $\text{CuAl}(\text{AsO}_4)\text{O}$ suggest that its quantum ground state can be represented as a collection of weakly interacting dimer units with the spin gap Δ of ~ 350 K on a distorted honeycomb lattice background, i.e., a valence-bond solid. The measurements of magnetic susceptibility in a wide temperature range have revealed pronounced deviation of experimental data from the fitting curves for both interacting and noninteracting dimer models. This deviation could be ascribed at least partially to the temperature expansion effects, which drastically change the intradimer exchange interaction parameter. The chemical decomposition effects prevent studies above $T^* = 800$ K. The range of study in the present paper is two times wider than the standard range of measurements, however. Therefore, the urusovite $\text{CuAl}(\text{AsO}_4)\text{O}$ can be considered a model compound to verify analytical and numerical expressions for the behavior of low dimensional magnetic systems.

ACKNOWLEDGMENTS

We thank P. S. Berdonosov for analysis of x-ray data of variously thermally treated samples and A. I. Smirnov for useful discussions. This paper was supported in part by the Ministry of Education and Science of the Russian Federation in the framework of the Increase Competitiveness Program of National University of Science and Technology “MISiS” (Grant No. K2-2014-036). The authors also acknowledge support of the Russian Foundation for Basic Research through Grants No. 13-02-00174, No. 14-02-00111, No. 14-02-00245, and No. 14-02-92693.

-
- [1] L. P. Vergasova, S. K. Filatov, M. G. Gorskaya, A. A. Molchanov, S. V. Krivovichev, and V. V. Ananiev, *Eur. J. Mineral.* **12**, 1041 (2000).
 - [2] A. A. Belik, H. J. Koo, M. H. Whangbo, N. Tsujii, P. Naumov, and E. Takayama-Muromachi, *Inorg. Chem.* **46**, 8684 (2007).
 - [3] E. Janod, L. Leonyuk, and V. Maltsev, *Solid State Comm.* **116**, 513 (2000).
 - [4] S. Lebernegg, A. A. Thirlin, O. Janson, and H. Rosner, *Phys. Rev. B* **88**, 224406 (2013).
 - [5] S. Lebernegg, A. A. Tsirlin, O. Janson, and H. Rosner, *Phys. Rev. B* **87**, 235117 (2013).
 - [6] H. Kikuchi, Y. Fujii, D. Takahashi, M. Azuma, Y. Shimakawa, T. Taniguchi, A. Matsuo, and K. Kindo, *J. Phys. Conf. Ser.* **320**, 012045 (2011).
 - [7] R. M. Krishna and S. K. Gupta, *Bull. Magn. Reson.* **16**, 239 (1994).
 - [8] F. Chabre, A. M. Ghorayeb, P. Millet, V. A. Pashchenko, and A. Stepanov, *Phys. Rev. B* **72**, 012415 (2005).
 - [9] G. A. Bain and J. F. Berry, *J. Chem. Educ.* **85**, 532 (2008).
 - [10] H. Lueken, *Magnetochemie* (Teubner, Leipzig, Germany, 1999).
 - [11] A. Tari, *The Specific Heat of Matter at Low Temperatures* (Imperial College Press, London, UK, 2003).
 - [12] D. D. Pollock, *Physical Properties of Materials for Engineers* (CRC Press, Boca Raton, USA, 1993).
 - [13] W. Kohn and L. J. Sham, *Phys. Rev.* **140**, A1133 (1965).
 - [14] J. P. Perdew, K. Burke, and M. Ernzerhof, *Phys. Rev. Lett.* **77**, 3865 (1996).
 - [15] P. W. Anderson, *Phys. Rev.* **79**, 350 (1950).
 - [16] O. K. Andersen and T. Saha-Dasgupta, *Phys. Rev. B* **62**, R16219 (2000).
 - [17] T. Mizuno, T. Tohyama, S. Maekawa, T. Osafune, N. Motoyama, H. Eisaki, and S. Uchida, *Phys. Rev. B* **57**, 5326 (1998).

- [18] O. S. Volkova, I. S. Maslova, R. Klingeler, M. Abdel-Hafiez, Y. C. Arango, A. U. B. Wolter, V. Kataev, B. Buechner, and A. N. Vasiliev, *Phys. Rev. B* **85**, 104420 (2012).
- [19] A. Vasiliev, O. Volkova, E. Zvereva, M. Isobe, Y. Ueda, S. Yoshii, H. Nojiri, V. Mazurenko, M. Valentyuk, V. Anisimov, I. Solovyev, R. Klingeler, and B. Buechner, *Phys. Rev. B* **87**, 134412 (2013).
- [20] M. M. Markina, B. V. Mill, E. A. Zvereva, A. V. Ushakov, S. V. Streltsov, and A. N. Vasiliev, *Phys. Rev. B* **89**, 104409 (2014).
- [21] S. Lebernegg, A. A. Tsirlin, O. Janson, and H. Rosner, *Phys. Rev. B* **89**, 165127 (2014).
- [22] K. V. Zakharov, E. A. Zvereva, P. S. Berdonosov, E. S. Kuznetsova, V. A. Dolgikh, L. Clark, C. Black, P. Lightfoot, W. Kockelmann, Z. V. Pchelkina, S. V. Streltsov, O. S. Volkova, and A. N. Vasiliev, *Phys. Rev. B* **90**, 214417 (2014).
- [23] V. P. Gupta and N. M. Ravindra, *Solid State Comm.* **32**, 1327 (1979).